IN-02
150327
P.13

NASA Technical Memorandum 107727

A GRIDLESS EULER/NAVIER-STOKES SOLUTION ALGORITHM FOR COMPLEX-AIRCRAFT APPLICATIONS

JOHN T. BATINA

FEBRUARY 1993

National Aeronautics and Space Administration

Langley Research Center
Hampton, Virginia 23681-0001

A GRIDLESS EULER/NAVIER-STOKES SOLUTION ALGORITHM FOR COMPLEX-AIRCRAFT APPLICATIONS

John T. Batina*
NASA Langley Research Center
Hampton, Virginia 23681-0001

Abstract

The development of a gridless computational fluid dynamics (CFD) method for the solution of the two- and three-dimensional Euler and Navier-Stokes equations is described. The method uses only clouds of points and does not require that the points be connected to form a grid as is necessary in conventional CFD algorithms. The gridless CFD approach appears to resolve the inefficiencies encountered with structured or unstructured grid methods, and consequently offers great potential for accurately and efficiently solving viscous flows about complex aircraft configurations. The method is described in detail and calculations are presented for standard Euler and Navier-Stokes cases to assess the accuracy and efficiency of the capability.

Introduction

Considerable progress in developing computational fluid dynamics (CFD) methods for aerodynamic analysis has been made over the past two decades.[1] The majority of work that has been done in CFD over the years has been on developing methods for use on computational grids that have an underlying geometrical structure and thus are referred to as "structured". For example, Fig. 1(a) shows a structured grid for the NACA 0012 airfoil. The grid is of C-type topology, has 159 points in the wraparound direction, and 49 points in the outward direction. Methods developed for structured grids have been applied to a wide variety of geometrical configurations ranging from simple analytically-defined airfoil sections such as the NACA 0012 airfoil to complex aircraft such as the F-16A fighter.[2] Although applications of structured grid methods to complex configurations are indeed possible they generally require more sophisticated meshing methodologies such as blocked, patched, chimera, or hybrid-type grids. For example, the F-16A fighter calculations reported in Ref. 2, which included the engine inlet and boundary layer diverter as well as the wing, fuselage, and tail in the geometrical modeling, used 27 blocks of structured cells to make up the grid. These more sophisticated meshing methodologies, in turn, significantly complicate the solution algorithms of the structured grid methods.

An alternative approach is the use of unstructured grids.[3-7] In two dimensions, unstructured grids typically are constructed from triangles, and in three dimensions, they consist of tetrahedral cells. The triangles or tetrahedra may be oriented in an arbitrary way to conform to the geometry, thus making it possible to easily generate grids about very complicated shapes. Although not a complicated shape, Fig. 1(b) shows an example of an unstructured grid for the NACA 0012 airfoil. The total grid has 3300 nodes and 6466 triangles. An advantage of methods developed for unstructured grids is that they may be applied to complex aircraft configurations without having to make changes to the basic solution algorithm. Numerous calculations for complex configurations performed using various Euler codes have been reported by several researchers.[3-7] However, applications to three-dimensional configurations using unstructured grid Euler codes have tended to be inefficient because the meshes have an excessively large number of cells. The excessive number of cells is due, in part, to the current state-of-the-art in generation of unstructured tetrahedral grids, which produces meshes that are much finer in the spanwise direction (for a given streamwise density) than is necessary for accurate flow computation. To alleviate the problem, the cells may be stretched in the spanwise direction when generating the mesh to reduce the number of cells. However, the stretching can create convergence and accuracy problems for the flow solver. The basic problem is that the tetrahedron is an inefficient geometrical shape (whereas the triangle tends to be an efficient shape in two dimensions). A more efficient shape for an isolated wing application is a prismatic cell defined by a polyhedron with a triangular cross-section. A mesh of this type uses triangles which form prisms when connected in the spanwise direction to grid the planes of the airfoil sections of the wing. This approach, though, not only puts structure back into the mesh, it is not generally applicable to complex three-dimensional configurations.

*Senior Research Scientist, Unsteady Aerodynamics Branch, Structural Dynamics Division. Associate Fellow, AIAA

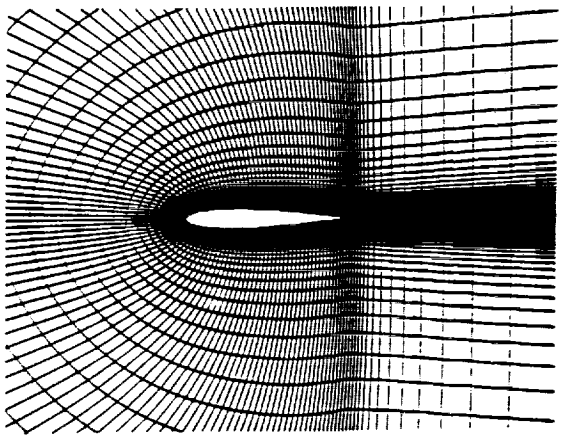

(a) structured.

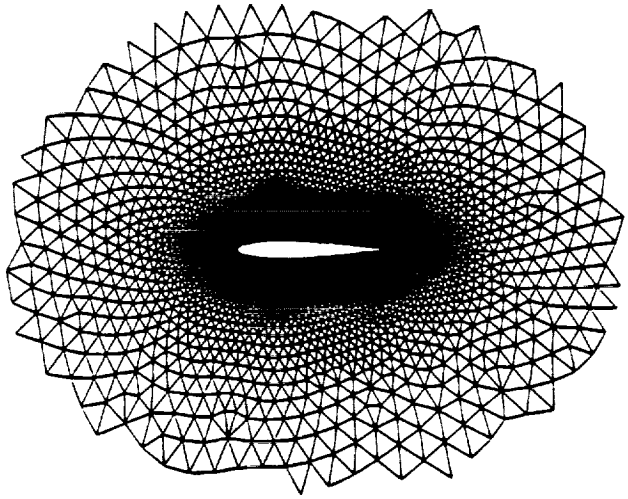

(b) unstructured.

Fig. 1 Partial view of meshes about the NACA 0012 airfoil.

Another problem with the unstructured-grid methodology is encountered in extending the methods for solving the Euler equations to the solution of the Navier-Stokes equations, especially in three dimensions. For viscous applications, grids generally need to be fine near the body in the outward direction to resolve the boundary layer but less fine in the direction along the surface of the body. This naturally leads to cells of high aspect ratio which tends to exacerbate the inefficiency of three-dimensional solution algorithms on tetrahedral meshes. Specifically, the use of tetrahedra for viscous flow applications results in an unreasonably large number of cells. The number of cells is in fact absurdly large in comparison to grids that are generated for Euler calculations (which are already inefficient because of a large number of cells as previously discussed) because of the additional requirement that the mesh be fine near the body. To alleviate this problem, a hybrid approach has been developed recently using prismatic cells for the solution of the Navier-Stokes equations.[8,9] In this approach, the surface of the geometry under consideration and the outer boundaries of the mesh are gridded using triangles, and instead of generating tetrahedra to fill the interior of the computational domain, the triangles on the inner and outer boundaries of the mesh are connected to form prisms.[8] The prisms, of course, require the same number of triangles on the inner and outer boundaries. While this hybrid approach is a viable solution to alleviate the inefficiency created by using tetrahedral cells to solve the Navier-Stokes equations, it is not necessarily the best approach, since it again puts structure back into the mesh and limits some of the advantages of the unstructured grid methodology, such as the ability to use spatial adaptation in regions of large flow gradients.

What is required to truly advance the CFD technology to treat complex configurations in viscous flows is not to take a step backward toward grid structure, but to take a bold step forward to develop methods that do not require the use of grids at all. Hence the solution to the above-mentioned problems with structured and unstructured grids is the development of algorithms for solving the Navier-Stokes equations based on using only grid points and not on the connectivity information that relates all of the points to one another. This type of approach, which may be referred to as "gridless" CFD, has distinct advantages over methods that require grids. Since only points are required, or specifically clouds of points as suggested by Chakravarthy,[10] gridless CFD methods offer the greatest potential for accurately and efficiently solving viscous flows about complex aircraft configurations. It is noted parenthetically, that if finally the grid points too were not required by the solution algorithm, then the ultimate flexibility in methodology could be attained. This type of method might then be referred to as "pointless" CFD.

The purpose of the paper it to report the development of a gridless method for the solution of the two- and three-dimensional Euler and Navier-Stokes equations. The method uses only clouds of points and does not require that the points be connected to form a grid as is necessary in conventional CFD algorithms. The governing partial differential equations (PDEs) are solved directly, by performing local least-squares curve fits in each cloud of points, and then analytically differentiating the resulting curve-fit equations to approximate the derivatives of the PDEs.[11] The method is neither a finite-difference nor a finite-volume type approach since differences, metrics, lengths, areas, or volumes are not computed. The method is described in further detail and calculations are presented for standard cases to assess the accuracy and efficiency of the capability.

Governing Equations

In this study the flow is assumed to be governed by the three-dimensional laminar Navier-Stokes equations which may be written in differential form as

$$\frac{\partial Q}{\partial t} + \frac{\partial}{\partial x}(E - E_v) + \frac{\partial}{\partial y}(F - F_v) + \frac{\partial}{\partial z}(G - G_v) = 0 \tag{1}$$

where Q is the vector of conserved variables given by

$$Q = \begin{Bmatrix} \rho \\ \rho u \\ \rho v \\ \rho w \\ e \end{Bmatrix}$$

E, F, and G are the inviscid fluxes in the x, y, and z directions, respectively, defined by

$$E = \begin{Bmatrix} \rho u \\ \rho u^2 + p \\ \rho uv \\ \rho uw \\ (e+p)\,u \end{Bmatrix}$$

$$F = \begin{Bmatrix} \rho v \\ \rho uv \\ pv^2 + p \\ \rho vw \\ (e+p)v \end{Bmatrix}$$

$$G = \begin{Bmatrix} \rho w \\ \rho uw \\ \rho vw \\ pw^2 + p \\ (e+p)w \end{Bmatrix}$$

and E_v, F_v, and G_v are the viscous fluxes in the x, y, and z directions, respectively, defined by

$$E_v = \begin{Bmatrix} 0 \\ \tau_{xx} \\ \tau_{xy} \\ \tau_{xz} \\ u\tau_{xx} + v\tau_{xy} + w\tau_{xz} - q_x \end{Bmatrix}$$

$$F_v = \begin{Bmatrix} 0 \\ \tau_{xy} \\ \tau_{yy} \\ \tau_{yz} \\ u\tau_{xy} + v\tau_{yy} + w\tau_{yz} - q_y \end{Bmatrix}$$

$$G_v = \begin{Bmatrix} 0 \\ \tau_{xz} \\ \tau_{yz} \\ \tau_{zz} \\ u\tau_{xz} + v\tau_{yz} + w\tau_{zz} - q_z \end{Bmatrix}$$

In the viscous fluxes the shear stresses and heat flux terms are defined by

$$\tau_{xx} = \frac{2}{3}\frac{M_\infty}{Re}\mu\left(2\frac{\partial u}{\partial x} - \frac{\partial v}{\partial y} - \frac{\partial w}{\partial z}\right)$$

$$\tau_{yy} = \frac{2}{3}\frac{M_\infty}{Re}\mu\left(2\frac{\partial v}{\partial y} - \frac{\partial u}{\partial x} - \frac{\partial w}{\partial z}\right)$$

$$\tau_{zz} = \frac{2}{3}\frac{M_\infty}{Re}\mu\left(2\frac{\partial w}{\partial z} - \frac{\partial u}{\partial x} - \frac{\partial v}{\partial y}\right)$$

$$\tau_{xy} = \frac{M_\infty}{Re}\mu\left(\frac{\partial u}{\partial y} + \frac{\partial v}{\partial x}\right)$$

$$\tau_{xz} = \frac{M_\infty}{Re}\mu\left(\frac{\partial w}{\partial x} + \frac{\partial u}{\partial z}\right)$$

$$\tau_{yz} = \frac{M_\infty}{Re}\mu\left(\frac{\partial v}{\partial z} + \frac{\partial w}{\partial y}\right)$$

$$q_x = -\frac{\gamma}{\gamma-1}\frac{M_\infty}{RePr}\mu\frac{\partial}{\partial x}\left(\frac{p}{\rho}\right)$$

$$q_y = -\frac{\gamma}{\gamma-1}\frac{M_\infty}{RePr}\mu\frac{\partial}{\partial y}\left(\frac{p}{\rho}\right)$$

$$q_z = -\frac{\gamma}{\gamma-1}\frac{M_\infty}{RePr}\mu\frac{\partial}{\partial z}\left(\frac{p}{\rho}\right)$$

In these equations, M_∞ is the freestream Mach number, Re is the Reynolds number, Pr is the Prandtl number, and μ is the molecular viscosity determined using Sutherland's law. The Euler equations are obtained by setting the viscous fluxes equal to zero; and the two-dimensional versions of the Euler or the Navier-Stokes equations are obtained by omitting the y–momentum equation and deleting all terms pertaining to the y-direction.

Spatial Discretization

Derivatives

The spatial derivatives in the governing equations (Eq. (1)) are approximated as follows. In each cloud of points, each term of the fluxes is assumed to vary linearly according to

$$f(x,y,z) = a_0 + a_1 x + a_2 y + a_3 z \qquad (2)$$

where the coefficients a_0, a_1, a_2, and a_3 are determined from a least-squares curve fit. Performing a least-squares fit in a given cloud results in four equations represented in matrix form by

$$\begin{bmatrix} n & \Sigma x_i & \Sigma y_i & \Sigma z_i \\ \Sigma x_i & \Sigma x_i^2 & \Sigma x_i y_i & \Sigma x_i z_i \\ \Sigma y_i & \Sigma x_i y_i & \Sigma y_i^2 & \Sigma y_i z_i \\ \Sigma z_i & \Sigma x_i z_i & \Sigma y_i z_i & \Sigma z_i^2 \end{bmatrix} \begin{Bmatrix} a_0 \\ a_1 \\ a_2 \\ a_3 \end{Bmatrix} = \begin{Bmatrix} \Sigma f_i \\ \Sigma x_i f_i \\ \Sigma y_i f_i \\ \Sigma z_i f_i \end{Bmatrix} \qquad (3)$$

where n is the number of points in the cloud and the summations are taken over the n points. The solution of Eqs. (3) requires the inversion of a 4 × 4 matrix which is performed for every cloud in the computational domain. Having solved these equations for a_0, a_1, a_2, and a_3, the spatial derivatives are now known since by differentiating Eq. (2) it is obvious that

$$\frac{\partial f}{\partial x} = a_1 \qquad \frac{\partial f}{\partial y} = a_2 \qquad \frac{\partial f}{\partial z} = a_3 \qquad (4)$$

Equations (3), however, are of the form

$$(A^T A)a = A^T f \qquad (5)$$

which can be troublesome numerically to solve since the matrix on the left-hand-side represented by A^TA may be ill conditioned.[12] It is more appropriate to solve the equations starting with

$$Aa = f \tag{6}$$

wherein the matrix A generally is not square. The solution procedure involves using a QR-decomposition to rewrite A as

$$A = QR \tag{7}$$

such that $Q^TQ = I$ (the identity matrix) and R is a square upper triangular matrix. Hence, the least squares problem now is defined as

$$QRa = f \tag{8}$$

or by pre-multiplying both sides of the equation by Q^T as

$$Ra = Q^Tf \tag{9}$$

The coefficients represented by a are solved then by simple back substitution (since R is an upper triangular matrix).

In addition to approximating the spatial derivatives of the governing equations by differentiation of the least-squares curve fits, the shear stresses and heat flux terms are calculated the same way. Since these terms involve first derivatives of the velocity components or pressure divided by density, the shear stresses and heat fluxes can be approximated by defining f to be equal to u, v, w, or p/ρ, and solving the least-squares problem. The resulting values for a_1, a_2, and a_3 are the derivatives of the specified quantity with respect to x, y, and z, respectively, within a given cloud of points.

Artificial Dissipation

The unsteady Euler equations are a set of nondissipative hyperbolic conservation laws that require some form of artificial dissipation to prevent oscillations near shock waves and to damp high frequency uncoupled error modes. The unsteady Navier-Stokes equations also require artificial dissipation for similar reasons because the physical viscosity generally is limited to the boundary layer. Since the method of the present work is conceptually analogous to a central-difference type approach, the artificial dissipation must be added explicitly to the solution procedure. This is accomplished by adding harmonic and biharmonic terms to the governing equations, corresponding to second and fourth differences of the conserved variables, respectively. These dissipation terms are defined by

$$D = \nabla\left(\epsilon^{(2)}\lambda\right)\nabla Q - \nabla^2\left(\epsilon^{(4)}\lambda\right)\nabla^2 Q \tag{10}$$

where λ is the local maximum eigenvalue of the governing equations, and $\epsilon^{(2)}$ and $\epsilon^{(4)}$ are local dissipation coefficients that are formulated similar to those of Jameson.[1] Furthermore, the above treatment of the artificial dissipation constitutes an isotropic dissipation model (independent of coordinate direction) which generally is only applicable to the Euler equations. For the Navier-Stokes equations, an anisotropic model is required due in part to the close spacing of points normal to the surface relative to the tangential distribution of points (analogous to high aspect ratio cells in structured or unstructured grid methods). Thus an anisotropic dissipation model was developed for use when solving the Navier-Stokes equations on clouds of points.

Temporal Discretization

Time Integration

The governing flow equations are integrated in time numerically using an explicit multi-stage Runge-Kutta time-stepping scheme.[1] Typically a four-stage scheme is used to solve the Euler equations with the artificial dissipation evaluated only during the first stage. A five-stage scheme is used to solve the Navier-Stokes equations with the artificial dissipation evaluated during the first, third, and fifth stages.

Residual Smoothing

The Runge-Kutta time-integration scheme described in the previous section has a step size that is limited by the Courant-Friedricks-Lewy (CFL) condition corresponding to CFL numbers of approximately 2.8 and 3.6 for the four-stage and five-stage schemes, respectively. To accelerate convergence to steady state, the CFL number may be increased by averaging the residual R with values at neighboring points.[1] This is accomplished by replacing R with the smoothed residual $\overline{R}$ given by

$$\overline{R} - \epsilon\nabla^2\overline{R} = R \tag{11}$$

where ϵ is a constant which controls the amount of smoothing and ∇^2 is an harmonic operator similar to that used in the dissipation model. Also similar to the dissipation model, an anisotropic form of the harmonic operator is used when solving the Navier-Stokes equations. Equation (11) is solved approximately using several Jacobi iterations. Convergence to steady state is further accelerated using enthalpy damping (only for the Euler equations) and local time stepping.

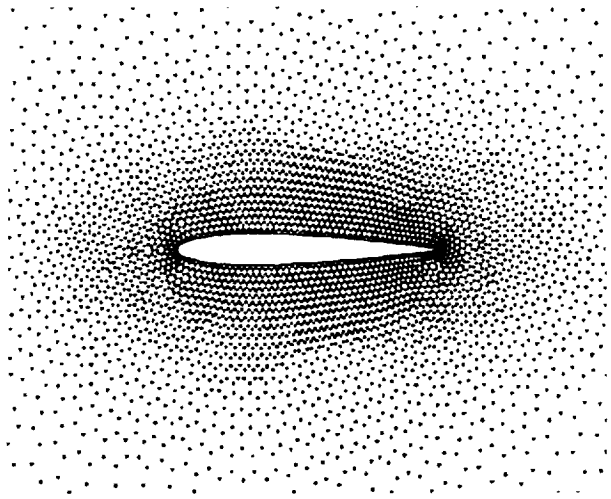

Fig. 2 Partial view of field of points about the NACA 0012 airfoil.

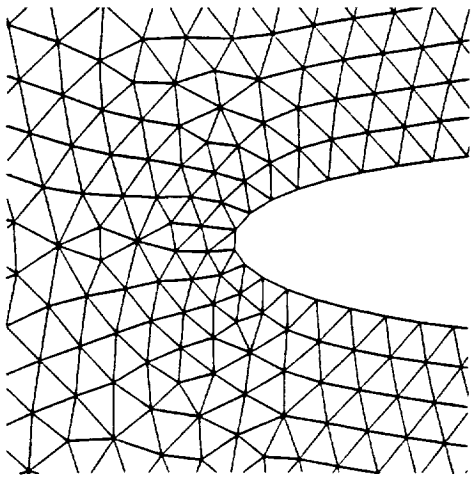

(a) unstructured mesh of triangles.

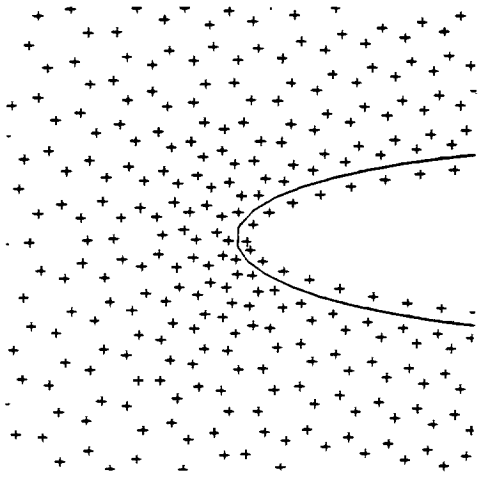

(b) corresponding field of points and ghost points for boundary conditions.

Fig. 3 Close-up view near the nose of the NACA 0012 airfoil.

Boundary Conditions

To impose the boundary conditions along the surface of the geometry being considered, ghost points that are located inside of the geometry are used. The locations of these ghost points are determined by a simple reflection of the flow field points that are close to the surface about the edges (2D) or faces (3D) that define the boundary. A similar procedure is used near the outer boundary to determine the locations of ghost points at which to impose the far-field boundary conditions.

Along solid surfaces, the velocity components at the ghost points are determined from the values at the corresponding flow field point adjacent to the surface. When solving the Euler equations, the velocity components at the ghost points are determined by imposing a flow tangency or slip condition which requires that the velocity normal to the surface vanishes. When solving the Navier-Stokes equations, the velocity components at the ghost points are determined by imposing a no-slip condition which simply changes the sign of the values of the components at the adjacent flow field points. In either case (Euler or Navier-Stokes), pressure and density at the ghost points are set equal to the values at the adjacent flow field points. Additional conditions are imposed using the ghost points to accurately treat the shear stresses and heat flux terms, as well as the artificial dissipation terms.

In the far field, a characteristic analysis based on Riemann invariants is used to determine the values of the inviscid flow variables at the ghost points that are located outside of the outer boundary. This analysis correctly accounts for wave propagation in the far field which is important for rapid convergence to steady state. Values of the viscous flow quantities at these ghost points are set equal to the values at the corresponding flow field points adjacent to the outer boundary.

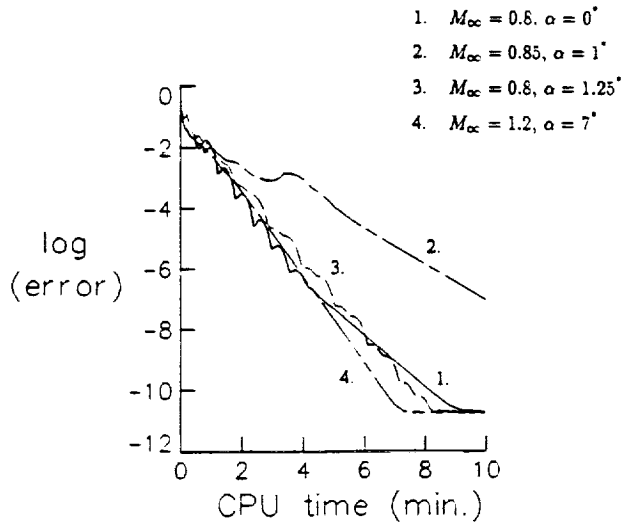

Fig. 4 Convergence histories from the gridless Euler solutions for the NACA 0012 airfoil.

Results and Discussion

Results are presented for standard Euler and Navier-Stokes cases to assess the accuracy and efficiency of the capability. All of the results were obtained using the Cray-YMP computer (Reynolds) at the Numerical Aerodynamic Simulation Facility located at the NASA Ames Research Center.

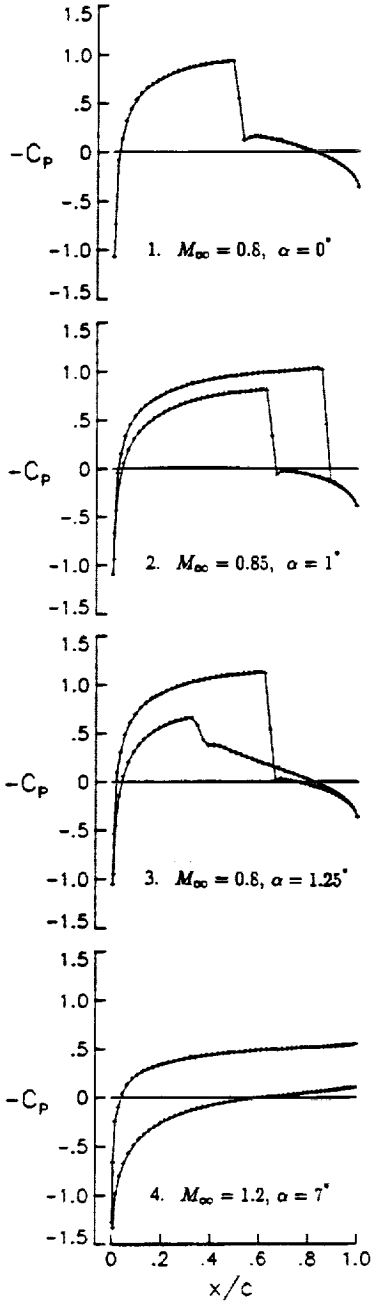

Fig. 5 Pressure distributions from the gridless Euler solutions for the NACA 0012 airfoil.

Two-Dimensional Results

Two-dimensional results were obtained first by solving the Euler equations for flows about the NACA 0012 airfoil. The field of points that was used to model the flow about the airfoil is plotted in Fig. 2. For convenience, the locations of these points were determined by using the cell centers from the unstructured grid of Fig. 1(b), and the cloud of points for each point was taken to be the cell centers of the three triangles that share edges with a given triangle. To more clearly demonstrate this, Fig. 3(a) shows a close-up view of the unstructured grid near the airfoil nose, and Fig. 3(b) shows the points determined from the cell centers. Figure 3(b) also shows ghost points that are located inside of the airfoil in order to impose the surface boundary conditions. The computational domain has a total of 6,500 points, 134 of which are ghost points. It is emphasized that the unstructured grid of Fig. 1(b) was used to determine the field of points of Fig. 2 only for convenience. In general, any method to determine the points is acceptable. Efficient generation procedures to determine clouds of points have yet to be developed.

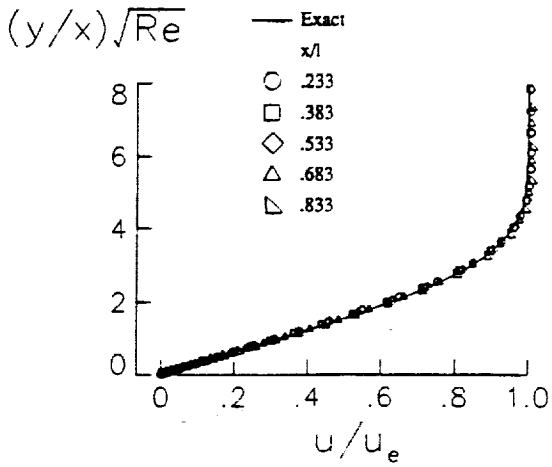

Fig. 6 Streamwise velocity distribution from the gridless Navier-Stokes solution for a flat plate at $M_\infty = 0.5$ and $Re = 10,000$.

Euler results were obtained using the points of Fig. 2 for four standard NACA 0012 airfoil cases corresponding to various combinations of freestream Mach number M_∞ and angle of attack α including: (1) $M_\infty = 0.8$, $\alpha = 0^\circ$; (2) $M_\infty = 0.85$, $\alpha = 1^\circ$; (3) $M_\infty = 0.8$, $\alpha = 1.25^\circ$; and (4) $M_\infty = 1.2$, $\alpha = 7^\circ$. All four cases were run using a CFL number of 5.0 with local time-stepping, residual smoothing, and enthalpy damping to accelerate convergence to steady state. Figure 4 shows the resulting convergence histories plotted as the log of the L_2-norm of the density residual versus the CPU time in minutes. The convergence histories indicate that convergence to steady state is obtained in only several minutes of CPU time; thus, the method is reasonably efficient in comparison with accepted runtimes of more conventional Euler methods (without multigrid acceleration). As further shown in Fig. 4, the slowest convergence is for case 2 ($M_\infty = 0.85$, $\alpha = 1^\circ$), which is because the solution contains two shock waves (upper and lower surfaces of the airfoil) of moderate strength. Therefore, it is slightly

harder to converge the solution of case 2 in comparison with the solutions of the other cases. Figure 5 shows the corresponding pressure coefficient distributions C_p versus the fractional chordlength x/c for the four NACA 0012 airfoil cases. The pressure distributions for cases 1, 2, and 3 indicate that the shock waves are sharply captured with only one interior point, which is somewhat surprising for a method that corresponds essentially to central differencing. The pressures for all four cases indicate that the generally-accepted Euler solutions have been obtained, which suggests that the gridless CFD method is accurate as well as efficient for such applications.

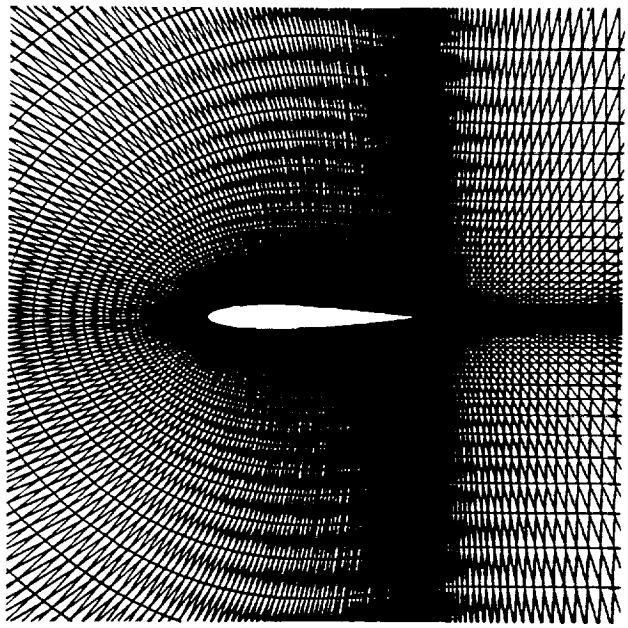

(a) unstructured mesh of triangles.

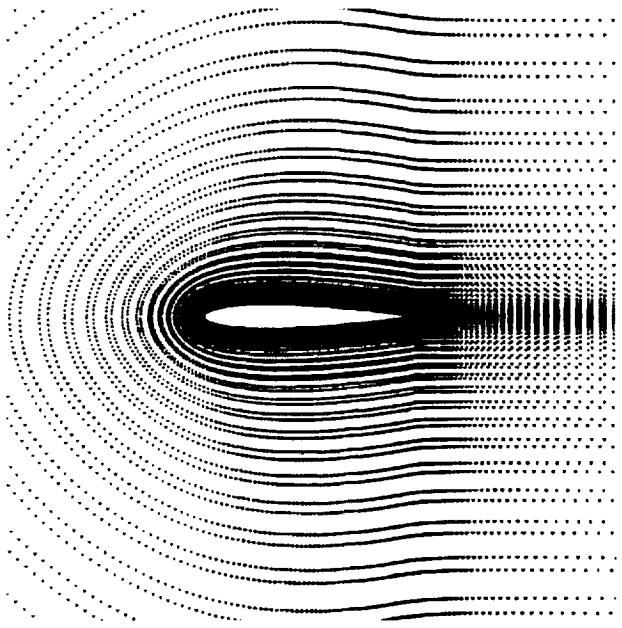

(b) corresponding field of points.

Fig. 7 Partial view of computational domains for the NACA 0012 airfoil.

Two-dimensional results were obtained next by solving the Navier-Stokes equations first for a flat plate and then for the NACA 0012 airfoil. For the flat plate, a solution was obtained initially to assess the gridless Navier-Stokes capability by making comparisons with the exact Blasius solution. The field of points that was used in these calculations was generated simply from a structured mesh of grid points, that were uniformly distributed along the flat plate, but clustered near the plate in the normal direction to resolve the boundary layer. The calculations were performed for $M_\infty = 0.5$ and $Re = 10,000$. The resulting streamwise velocity component u (normalized by the freestream value u_e), plotted versus the similarity variable $(y/x)\sqrt{Re}$, is shown in Fig. 6 at $x/l = 0.233,\ 0.383,\ 0.533,\ 0.683$, and 0.833. The gridless results, represented by the symbols, indicate that the similarity solution for a flat plate boundary layer is correctly obtained, and that the solution agrees well with the Blasius solution.

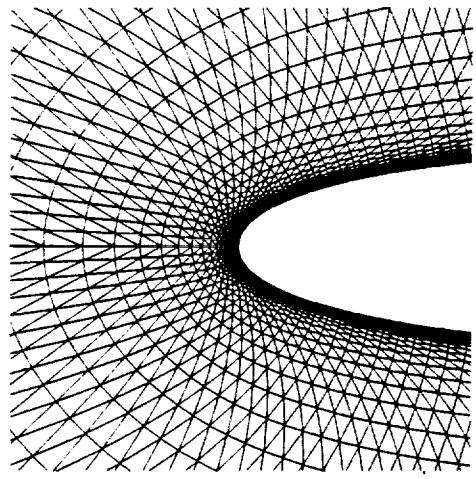

(a) unstructured mesh of triangles.

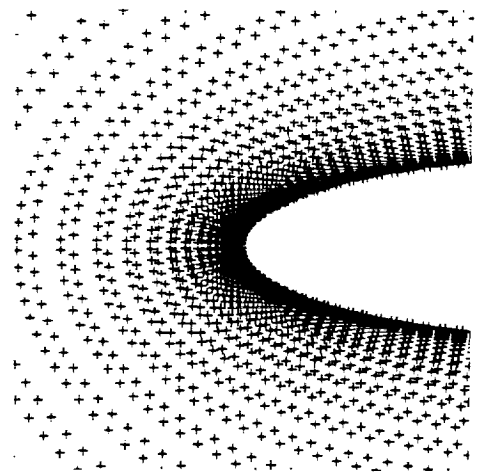

(b) corresponding field of points.

Fig. 8 Close-up view near the nose of the NACA 0012 airfoil.

Navier-Stokes results also were obtained for a standard laminar case for the NACA 0012 airfoil corresponding to $M_\infty = 0.5$, $\alpha = 0^\circ$, and $Re = 5000$. Again the

field of points that was used to model the flow about the airfoil was determined for convenience by using the cell centers from an unstructured grid of triangles. A partial view of the unstructured grid is shown in Fig. 7(a) (generated from a structured grid of C-type topology), and the corresponding view of points for the gridless method is shown in Fig. 7(b). Close-up views near the airfoil nose of the unstructured grid and the gridless field of points are shown in Figs. 8(a) and 8(b), respectively. The computational domain in the latter case has a total of 30,720 points, 608 of which are ghost points. Navier-Stokes

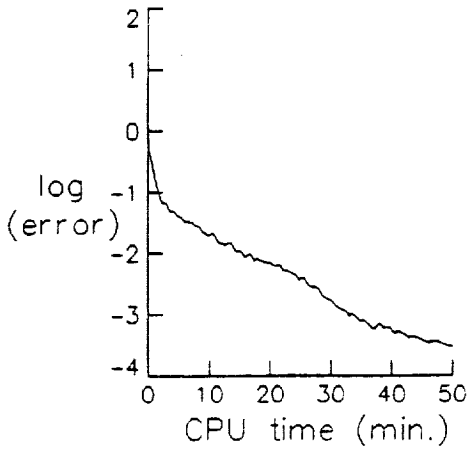

(a) convergence history.

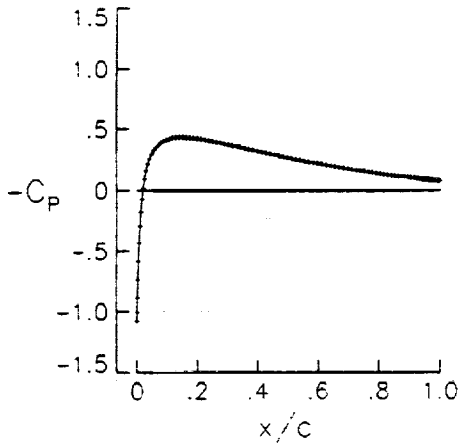

(b) pressure distribution.

Fig. 9 Gridless Navier-Stokes solution for the NACA 0012 airfoil at $M_\infty = 0.5$, $\alpha = 0^\circ$, and $Re = 5000$.

results were obtained using a CFL number of 4.0 with local time-stepping and residual smoothing to accelerate convergence to steady state. Figure 9(a) shows the resulting convergence history plotted as the log of the L_2-norm of the density residual versus the CPU time in minutes. The convergence history indicates that acceptable convergence is obtained in less than one hour of CPU time which is reasonable considering that the method does not currently use multigrid to accelerate convergence to steady state. Figure 9(b) shows the corresponding pressure distribution which indicates that the generally-accepted Navier-Stokes solution involving separated flow near the trailing edge has been obtained by using the gridless CFD method. To more clearly see the flow solution in the trailing-edge region, velocity vectors are presented in Fig. 10. The flow separates near 82% chord along the upper and lower surfaces of the airfoil, and the velocity vectors indicate that there are small recirculation bubbles downstream of the trailing edge. This solution is consistent with the Navier-Stokes solutions reported by other researchers obtained for this case using structured (Ref. 13) and unstructured (Ref. 14) grids.

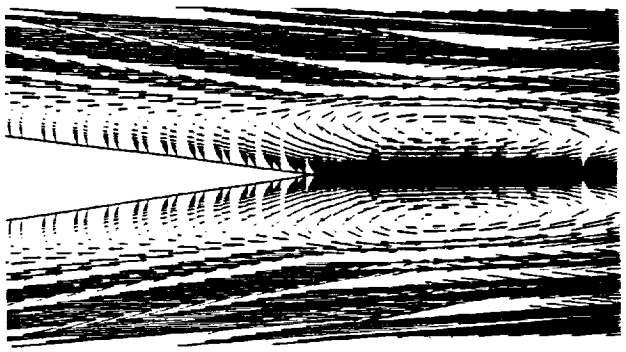

Fig. 10 Velocity vectors near the trailing edge of the NACA 0012 airfoil at $M_\infty = 0.5$, $\alpha = 0^\circ$, and $Re = 5000$.

Three-Dimensional Results

Three-dimensional results were obtained first for the two-dimensional cases that were presented in the previous section. The computational domains in 3D were created from the 2D fields of points ($y = 0.0$) by using two additional planes of points at $y = \pm 1.0$. The points in these planes were taken to be additional ghost points that were used to impose symmetry conditions on either side of the flow field points and effectively produce two-dimensional solutions. The 3D calculations for the 2D cases agreed to plotting accuracy with the 2D results and, hence, are not presented here.

Results were obtained next for the ONERA M6 wing[15] for $M_\infty = 0.84$ and $\alpha = 3.06^\circ$. This case is an AGARD standard case for the assessment of inviscid flowfield methods,[15] where experimental steady pressure data are available for comparison with calculated pressures. The M6 wing has a leading edge sweep angle of 30°, an aspect ratio of 3.8, and a taper ratio of 0.562. The airfoil section of the wing is the ONERA "D" airfoil which is a 10% maximum thickness-to-chord ratio conventional section. The results were obtained using a field of points that was created for convenience from an existing unstructured mesh of tetrahedra.[16] The locations of the points were determined by using the cell centers of the tetrahedra, and the cloud of points for each point was taken to be the cell centers of the four tetrahedra that share faces with a given tetrahedron. The computational domain has a total of 108,705 points, 10,388 of which are ghost points. The ghost points that are used to model the surface of the wing and the symmetry plane

are shown in Figs. 11 and 12, respectively. These ghost points are not distributed in an optimal way since the points are too coarse in the stream direction (leading to possible inaccuracy due to too few points) and too fine in the span direction (leading to inefficiency due to unnecessary points). This is a consequence of using an unstructured tetrahedral mesh to create the field of points to test the gridless method. Nonetheless, it allows an adequate test of the method, although, in the future, better fields of points will be generated to exploit the advantages of the gridless approach. Figure 13 shows surface pressure coefficient comparisons with the experimental data at the $\eta = 0.2$, 0.44, 0.65, and 0.9 span stations. In these plots the Euler results are given by the solid curves where plus signs have been included to indicate the actual ghost point values, near the particular span station, which are connected with straight line segments. The experimental data is represented by the circles. For $\eta = 0.2$, shown in Fig. 13(a), there are two shock waves along the chord. The forward shock wave is well predicted. The second shock wave is predicted slightly downstream of the experimental shock location which is typical of inviscid methods for this case. Also, the lower surface pres-

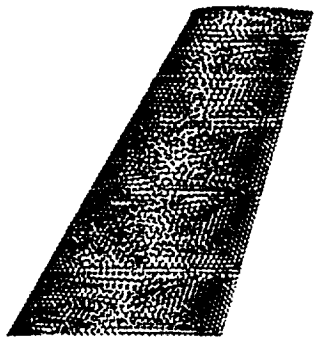

Fig. 11 Ghost points for upper surface of the ONERA M6 wing.

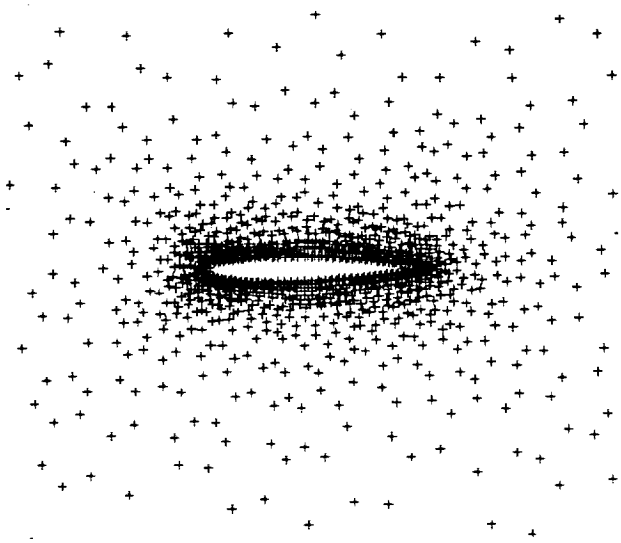

Fig. 12 Ghost points for symmetry plane of the ONERA M6 wing.

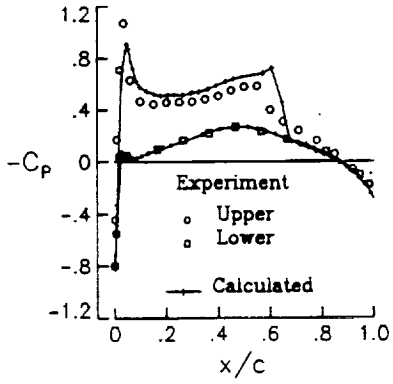

(a) $\eta = 0.2$.

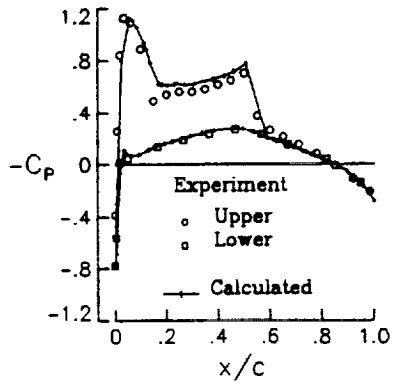

(b) $\eta = 0.44$.

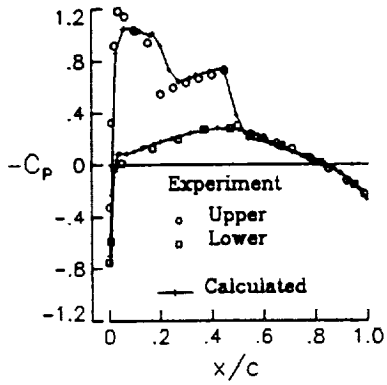

(c) $\eta = 0.65$.

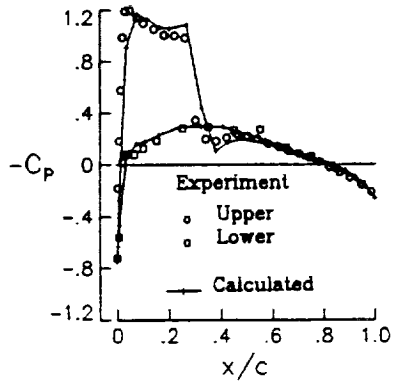

(d) $\eta = 0.9$.

Fig. 13 Comparison of calculated and experimental pressure coefficients for the ONERA M6 wing at $M_\infty = 0.84$ and $\alpha = 3.06°$.

sure coefficients agree well with the data. At $\eta = 0.44$, shown in Fig. 13(b), the shock locations have begun to coalesce. The leading edge suction peak is well predicted and both shock waves are captured sharply. At $\eta = 0.65$, shown in Fig. 13(c), the forward shock wave near 20% chord is predicted to be downstream of the experimental location and the second shock wave is near midchord. Furthermore, the lower surface pressure coefficients are predicted accurately. At $\eta = 0.9$, shown in Fig. 13(d), the two shocks have merged to form a single, relatively strong, shock wave near 25% chord. Here the shock is sharply captured and the calculated pressures again agree reasonably well with the experimental data. Finally, the gridless results of Fig. 13 are of comparable accuracy in comparison with results obtained using an unstructured grid method for this case.[16]

Concluding Remarks

The development of a gridless CFD method for the solution of the two- and three-dimensional Euler and Navier-Stokes equations was described. The method uses only clouds of points and does not require that the points be connected to form a grid as is necessary in conventional CFD algorithms. The gridless CFD approach appears to resolve the inefficiencies encountered with structured or unstructured grid methods, and, consequently, offers great potential for accurately and efficiently solving viscous flows about complex aircraft configurations. The method was described in detail and calculations for standard cases were presented to assess the accuracy and efficiency of the capability. The capability was tested for the solution of the Euler equations and for the solution of the laminar Navier-Stokes equations. These solutions were found to be reasonably accurate and efficient in comparison with solutions from conventional CFD methods.

The gridless method is not faster on a per point basis in comparison with advanced methods developed for structured or unstructured grids. (For example, the 3D Euler code required approximately 27μs/iteration/point and the 3D Navier-Stokes code requires approximately 35μs/iteration/point.) The advantage of the gridless method is that it allows the use of fields of points where the points are more appropriately located and clustered, leading to far fewer points to solve a given problem in comparison with an unstructured grid method. This advantage may be realized while retaining the advantages of the unstructured grid method, namely, general-geometry treatment in a single-block computational domain, and ease in implementing a spatial adaptation capability. A disadvantage of the gridless approach, though, is that it requires an indirect addressing system to point from clouds to points, similar to the indirect addressing used by unstructured grid methods. (The 3D Euler/Navier-Stokes code requires approximately 82 array locations/point.) However, the memory overhead that the indirect addressing produces is quite small in comparison to the memory savings that can be realized by using fewer points.

Finally, conservation of mass, momenta, and energy is a concern for the gridless approach since this is an obviously desirable property for any numerical method for the solution of the Euler or Navier-Stokes equations. The current gridless method solves the conservation law form of these equations but it is not clear that the method is conservative, at least not in the same sense as conservative finite-volume methods. In a finite-volume method, the flux out of one cell is the identical flux into the next cell through the common face, and hence conservation is ensured. However, the gridless approach is more like a finite-element (FE) method with some aspects of a finite-difference (FD) method. Consequently, the gridless approach is expected to have similar properties with respect to the conservation issue as FE and FD methods. Nonetheless, this question requires further investigation.

References

1. Jameson, A., "Successes and Challenges in Computational Aerodynamics," AIAA Paper 87-1184, Jan. 1987.
2. Flores, J. and Chaderjian, N. M., "Zonal Navier-Stokes Methodology for Flow Simulation About a Complete Aircraft," *Journal of Aircraft*, Vol. 27, July 1990, pp. 583–590.
3. Jameson, A., Baker, T. J., and Weatherill, N. P., "Calculation of Inviscid Transonic Flow over a Complete Aircraft," AIAA Paper 86-0103, Jan. 1986.
4. Peraire, J., Peiro, J., Formaggia, L., and Morgan, K., "Finite Element Euler Computations in Three Dimensions," AIAA Paper 88-0032, Jan. 1988.
5. Lohner, R., and Baum, J. D., "Numerical Simulation of Shock Interaction with Complex Geometry Three-Dimensional Structures Using a New Adaptive H-Refinement Scheme on Unstructured Grids," AIAA Paper 90-0700, Jan. 1990.
6. Frink, N. T., Parikh, P., and Pirzadeh, S., "Aerodynamic Analysis of Complex Configurations Using Unstructured Grids," AIAA Paper 91-3292, Sept. 1991.
7. Batina, J. T., "A Fast Implicit Upwind Solution Algorithm for Three Dimensional Unstructured Dynamic Meshes," AIAA Paper 92-0447, Jan. 1992.
8. Nakahashi, K., "A Finite-Element Method on Prismatic Elements for the Three-Dimensional Navier-Stokes Equations," *Lecture Notes in Physics*, Vol. 323, 1989, pp. 434–438.
9. Kallinderis, Y., "Prismatic Grid Generation with an Efficient Algebraic Method for Aircraft Configurations," AIAA Paper 92-2721, June 1992.
10. Chakravarthy, S. R., "Some New Approaches to Grid Generation, Discretization, and Solution Methods for CFD," presented at the 4th International Symposium

on Computational Fluid Dynamics, Davis, California, Sept. 9–12, 1991.

11. Batina, J. T., "A Gridless Euler/Navier-Stokes Solution Algorithm for Complex Two-Dimensional Applications," NASA TM-107631, June 1992.

12. Anderson, W. K., Personal Communication, June 1992.

13. Radespiel, R., and Swanson, R. C., "An Investigation of Cell Centered and Cell Vertex Multigrid Schemes for the Navier-Stokes Equations," AIAA Paper 89-0543, Jan. 1989.

14. Mavriplis, D. J., Jameson, A., and Martinelli, L., "Multigrid Solution of the Navier-Stokes Equations on Triangular Meshes," ICASE Report No. 89-11, Feb. 1989.

15. Schmitt, V., and Charpin, F., "Pressure Distribution on the ONERA M6 Wing at Transonic Mach Numbers," Appendix B1 in AGARD-AR-138, Experimental Data Base for Computer Program Assessment, May 1979.

16. Woodard, P. R., Batina, J. T., and Yang, H. T. Y., "Quality Assessment of Two- and Three-Dimensional Unstructured Meshes and Validation of an Upwind Euler Flow Solver," AIAA Paper 92-0444, Jan. 1992.

REPORT DOCUMENTATION PAGE

Form Approved
OMB No. 0704-0188

1. AGENCY USE ONLY *(Leave blank)*	2. REPORT DATE	3. REPORT TYPE AND DATES COVERED
	February 1993	Technical Memorandum

4. TITLE AND SUBTITLE
A Gridless Euler/Navier-Stokes Solution Algorithm for Complex-Aircraft Applications

5. FUNDING NUMBERS
505-63-50-12

6. AUTHOR(S) John T. Batina

7. PERFORMING ORGANIZATION NAME(S) AND ADDRESS(ES)
NASA Langley Research Center
Hampton, VA 23681-0001

8. PERFORMING ORGANIZATION REPORT NUMBER

9. SPONSORING / MONITORING AGENCY NAME(S) AND ADDRESS(ES)
National Aeronautics and Space Administration
Washington, DC 20546-0001

10. SPONSORING / MONITORING AGENCY REPORT NUMBER
NASA TM 107727

11. SUPPLEMENTARY NOTES
Paper Presented at the AIAA 31st Aerospace Sciences Meeting, Reno, Nevada, January 11-14, 1993.

12a. DISTRIBUTION / AVAILABILITY STATEMENT
Unclassified - Unlimited
Subject Category 02

12b. DISTRIBUTION CODE

13. ABSTRACT ***(Maximum 200 words)***

The development of a gridless computational fluid dynamics (CFD) method for the solution of the two- and three-dimensional Euler and Navier-Stokes equations is described. The method uses only clouds of points and does not require that the points be connected to form a grid as is necessary in conventional CFD algorithms. The gridless CFD approach appears to resolve the inefficiencies encountered with structured or unstructured grid methods, and consequently offers great potential for accurately and efficiently solving viscous flows about complex aircraft configurations. The method is described in detail and calculations are presented for standard Euler and Navier-Stokes cases to assess the accuracy and efficiency of the capability.

14. SUBJECT TERMS
Computational Fluid Dynamics
Numerical Analysis
Transonic Flow
Viscous Flow

15. NUMBER OF PAGES
12

16. PRICE CODE
A03

17. SECURITY CLASSIFICATION OF REPORT	18. SECURITY CLASSIFICATION OF THIS PAGE	19. SECURITY CLASSIFICATION OF ABSTRACT	20. LIMITATION OF ABSTRACT
Unclassified	Unclassified	Unclassified	